UNIVERSITY OF MISKOLC
MIKOVINY SÁMUEL DOCTORAL SCHOOL OF EARTH SCIENCES
Head of the doctoral school:
Prof. Péter Szűcs, PhD

MINERAL PARAGENESES OF ANTIMONY AS A CRITICAL RAW MATERIAL IN HUNGARY

Thesys book of the doctoral dissertation

MADE BY:
Richárd Zoltán Papp
geologist engineer

SUPERVIZOR:
Dr. Norbert Zajzon, PhD
associate professor

May 2022

1. Introduction, objectives

Antimony is a geochemically rare element in the earth's crust, with an average content of 0.65 ppm (Dill, 2010), making deposits as small as 30 000 tons for significant deposit. There are a total of 3 giants worldwide, each with assets in excess of 300,000 tons (Xikuangshan, China; Bolivian Sb-belt; Kadamzhai, Tajikistan), and 21 smaller but significant deposits are known worldwide (Móricz, et al., 2013).

Due to its various uses, it is a critical element for the European Union, mainly as a key substance for the production of solar cells.

One of the main objectives of this research was to investigate the antimony-bearing minerals and their paragenesis from different deposits in Hungary (**Figure 1**), to use the results to refine the genetics of the Hungarian deposits and to publish the data available to support the exploration if new ore deposits worldwide. Knowledge about the occurring sulphosalt minerals is essential to elaborate an accurate and detailed paragenetic picture and to acertain the deposit. For this reason, one of the most important objectives of my work was to investigate the sulphosalt minerals in the selected locations, as – due to the complexity of the subject, the difficulty to reach proper instrumentation and the small number of available samples – no such research has been carried out in Hungary for many decades.

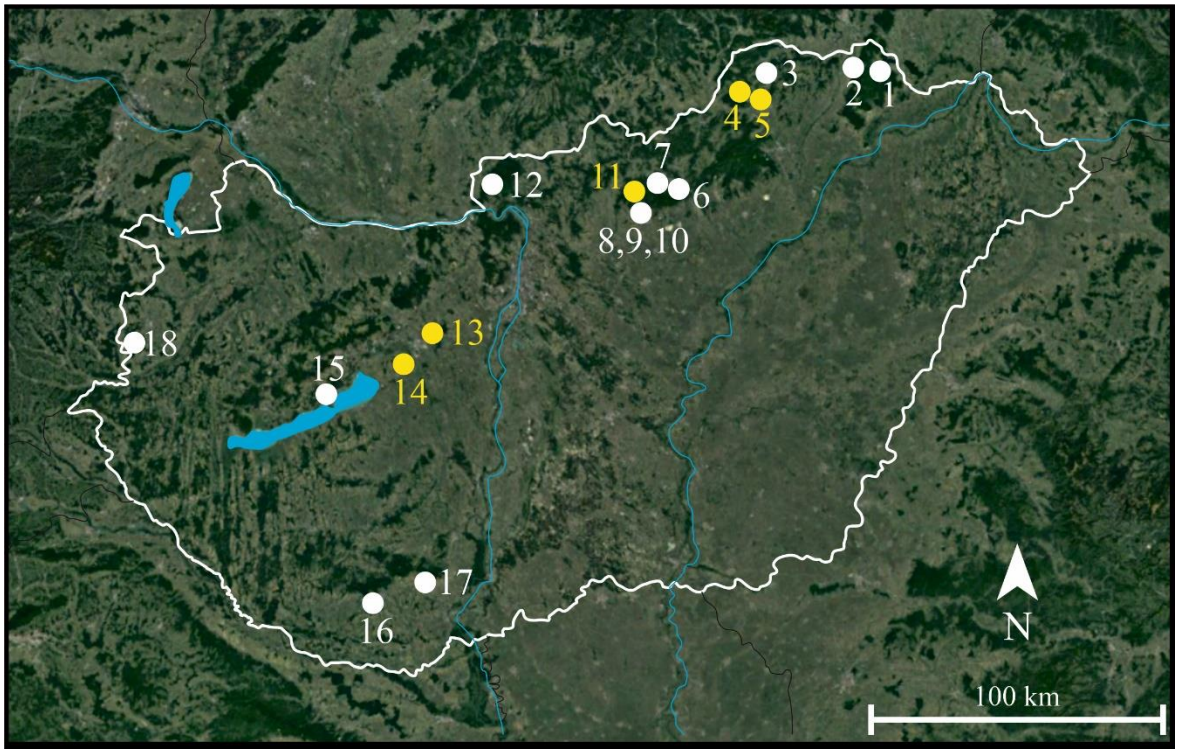

1. Figure - Occurrences of sulphosalt minerals in Hungary (Papp & Zajzon, 2018)
(1: Füzérradvány, 2: Telkibánya, 3: Tornaszentandrás, 4: Rudabánya, 5: Martonyi, 6: Recsk, 7: Parádfürdő, 8: Gyöngyösoroszi, 9: Károlytáró, 10: Gyöngyössolymos, 11: Mátraszentimre, 12: Nagybörzsöny, 13: Velencei-hegység, 14: Szabadbattyán, 15: Balatonfüred, 16: Erdősmecske, 17: Kővágószőlős, 18: Felsőcsatár
The locations marked in yellow were investigated in this research.

Since sulphosalts are a very complex and diverse group of minerals, I preferred to identify the antimony-bearing phases, which I determined on the basis of the latest scientific results.

During my PhD research, I determined the antimony-bearing mineral assemblages of five Hungarian deposits (Meleg hill – Velence Mountains, Szabadbattyán, Mátraszentimre, Rudabánya, Martonyi) with a special focus on sulphosalt minerals (Papp & Zajzon, 2018) (**Figure 1**). Using the data obtained, my work aimed to clarify the genetics of the deposits, search for analogies in the Carpathian and Alpine ranges (Benkó, et al., 2010; 2014a; 2014b; Hargitainé Molnár, 2019), and look for relationships between the different domestic ore deposits.

2. Methods used

During the research, scanning electron microscopy was used with an energy dispersive (EDX) spectrometer to determine most of the phases present after preliminary stereomicroscopic and reflect light optical microscopic observations of the samples. This technology allows very fast measurements but has the disadvantage that it is not always possible to determine the exact chemical composition. This is due to the characteristic peaks of the elements within the spectrum under investigation have similar energies and the resulting peaks overlap, like the peaks of sulphur-lead-bismuth. Since these are enriched in the ore deposits I have studied, and also occur together preferentially in the minerals studied, a method had to be chosen to separate these elements from each other and thus to perform an accurate quantitative analysis.

Electron microprobe analysis (EPMA) allows measurements with much better energy resolution, usually using multiple wavelength dispersive (WDX) spectrometers simultaneously. The disadvantage is that only one element can be measured at a time with one spectrometer. Increasing number of elements to be analysed expand the measurement time, which could lead to inaccurate data in the presence of certain volatile components and unstable phases due to electron beam effects.

Due to the complexity and time-consuming nature of the WDX measurements, I primarily used EDX to measure the phases in my samples, and after that WDX measurements have been only performed on certain pre-selected minerals. Thus, during my work nearly 10,000 EDX measurements were made and approximately 400 WDX analyses were performed.

Confirming the results obtained by EPMA some samples were also measured by Raman spectroscopy.

The electron microscopic investigations were mainly obtained at the University of Miskolc (ME), part of the WDX measurements at the Dionýz Štúr Geological Institute (DSGI) in Bratislava, and the Raman spectroscopy at the Raman laboratory in the Department of Mineralogy of Eötvös Loránd University (ELTE-TTK). Measurements performed:

- Stereo- and Reflected light microscopy (ME)
- Focused Plasma Beam Scanning Electron Microscopy (PFIB-SEM) (ME)
- Electron probe microanalysis (EPMA) (ME, DSGI)
- Raman spectroscopy (ELTE-TTK)

During the sample preparation, polished surface mounts were made. After the samples were vacuum impregnated in Araldite epoxy resin, they were cut and their surface was ground under dry condition on SiC abrasive paper and polished with diamond paste (6 μm, 3 μm, 1

μm, 1/4 μm) under wet condition (alcohol-based lubricant was used to avoid any oxidation of the sample surface during the process).

Electron microprobe measurements were performed on a JEOL JXA-8600 Superprobe with upgraded SAMX control, 20 kV acceleration voltage and 20 nA beam current (Miskolc) and with a Cameca SX-100 microprobe with 25 kV acceleration voltage and 10 nA beam current (Bratislava). Table I. contains the analyser crystal types and standards that were used during the WDX measurements.

The SEM images were taken with a Thermo Scientific Helios G4PFIB XCe, Xe Plasma Focused Ion Beam Scanning Electron Microscope, equipped with an EDAX Team Pegasus system (Octane detector), with 15–20 kV acceleration voltage and 3.2–13 nA beam current. The acceleration voltage and the beam current were modified according to the method of use (imaging or chemical measurement).

1. Table - The applied analysing crystals and standards for the measured elements (normal letter: University of Miskolc; *italic letter: Geological Institute of Dionýz Štúr*).

Element	**Anal. crystal**	**Standard**
As Lα	TAP/*TAP*	GaAs/*GaAs*
Ag Lα	PET/*LPET*	Ag/*Ag*
S Kα	PET/*LPET*	MnS_2/*$CuFeS_2$*
Cu Lα/*Kα*	TAP/*LLIF*	Cu_3Se_2/*$CuFeS_2$*
Sb Lα	PET/*LLIF*	Sb_2S_3/*Sb*
Bi Mα/*Lα*	PET/*LLIF*	Bi/*Bi*
Fe Kα	LIF/*LLIF*	FeS_2/*$CuFeS_2$*
Pb Mα	PET/*LPET*	PbS/*PbS*
Zn Lα/K*α*	TAP/*LLIF*	Zn/*ZnS*
Hg Lα	LIF/*LLIF*	HgS/*HgS*

Raman spectroscopic data were obtained with a HORIBA Jobin Yvon LabRAM HR UV-vis-NIR confocal Raman microspectrometer coupled to an Olympus BXFM microscope. For excitation the 532 nm emission of a frequency-doubled Nd:YAG laser has been used, focused on the sample with a 100x (0.9 NA) objective. The focal length of the spectrograph was 800 mm, and the 1800 grooves/mm optical grating was used. Spectral calibration was done for the Rayleigh line and zero-order reflection of the grating.

Among the sulphosalt minerals, I payed special attention to the mineral(s) referred in the Hungarian literature as "andorite" (Krenner, 1892; Krenner, 1894). According to the present state of science-„andorite” can be divided into at least two distinct phases: andorite IV and VI (formerly called quatrandorite and senandorite (Sawada, et al., 1987)).

Andorite series minerals are the Sb-rich members of the lillianite homologous series. Those minerals are complex sulphides with Pb-Bi-Sb-Ag-S chemistry. The crystal structure of the lillianite series is built up from alternating layers of PbS parallel to the $(311)_{PbS}$ lattice plane.

In the case of the andorite-series minerals, under- and oversubstitution can be observed by the replacement of the Pb atom in these alternating PbS layers.

For our calculations, we used the work of Makoviczky és Karup-Møller (1977a; 1977b) about the classification of the lillianite series, which is based on the lillianite homologue, the molar fraction and the substitution percentage of the phases.

The andorite homologue value (N) was calculated with the following equation:

$$N= – 1 + 1 / (Sbi + Pbi / 2 – 1 / 2) \quad (1)$$

where Sbi = Sb / (Ag + Sb + Pb) Pbi = Pb / (Ag + Sb + Pb); Sb = Sb + Bi + As; Ag = Ag + Cu and Pb = Pb + Zn + Hg + Cd (MOËLO et al. 1984; MAKOVICKY 2019).

The substitution percentage (L%) of the Ag-Sb end member of the andorite is equal to

$$L\% = 1 – (2Sbi – Pbi – 1) / 6 * (Bi + Pbi / 2 – 5 / 6) * 100 \quad (2)$$

and the substitution parameter is:

$$x = (L\% * (N – 2)) / 200 \quad (3)$$

The equations were calculated with the chemical formula of andorite VI ($PbAgSb_3S_6$).

The andorite series comprises well-defined minerals with limited composition ranges and limited content of specific minor elements. The substitution percentages of the andorite-series minerals can be seen in **Table 2**. Due to the continuous under- and oversubstitution of the specimens in nature, the substitution percentage can be described as a continuous range between the two neighbouring mineral species.

N and L values were calculated for selected members of the andorite series from different localities based on analytical data taken from earlier publications (Makovicky & Karup-Møller, 1977a; 1977b; 1977c; Kostov & Minčeva-Stefanova, 1981; Moëlo, et al., 2008; Ozdín & Sejkora, 2009; Pršek, et al., 2009).

2. Table -Minerals of the andorite-series with their chemical composition, space group, substitution percentage (L%) and andorite homologue order value (N) (Moëlo, et al., 2008; Pažout, 2017)

Name	**Chemical composition**	**Space group**	**L%**	**N**
uchucchacuaite	$Pb_3MnAgSb_5S_{12}$	*Pmmm*	And_{50}	4
fizélyite	$Ag_5Pb_{14}Sb_{21}S_{48}$	*P2₁/n*	$And_{62.5}$	4
ramdohrite	$(Cd,Mn,Fe)Ag_{5.5}Pb_{12}Sb_{21.5}S_{48}$	*P2₁/n*	$And_{68.75}$	4
andorite IV	$Ag_{15}Pb_{18}Sb_{47}S_{96}$	*P2*	$And_{93.75}$	4
andorite VI	$AgPbSb_3S_6$	*Pmn2₁*	And_{100}	4
arsenquatrandorite	$Pb_{12.8}Ag_{17.6}Sb_{38.08}As_{11.52}S_{96}$	*P2₁/b*	And_{110}	4
roshchinite	$Pb_{10}Ag_{19}Sb_{51}S_{96}$	*Pnma*	And_{115}	4
oscarkempffite	$Pb_4Ag_{10}Sb_{17}Bi_9S_{48}$	*Pnca*	And_{124}	4
clino-oscarkempffite	$Pb_6Ag_{15}Sb_{21}Bi_{18}S_{72}$	*P2₁/b*	And_{125}	4
jasrouxite	$Pb_4Ag_{16}Sb_{24}As_{16}S_{72}$	*P-1*	$And_{136.5}$	4

3. Investigated samples

During my work, I examined a total of 20 polished surface block samples enclosing 36 rock pieces in which I found antimony-bearing phases. In addition to these, 15 samples were prepared and measured which subsequently did not contain any phases relevant to my thesis, so I will not discuss their results here. **Table 3** lists the samples and the applied analytical methods.

3. Table - Unique IDs of the samples and list of investigations carried out on them

	Sample ID	**Optical microscope**	**PFIB-SEM**	**SEM-EDX**	**EPMA EDX**	**EPMA WDX**	**Bratislava WDX**	**Raman**
1	Polyanka 2019	X	X		X		X	
2	Rb-A-I Szfalerit		X	X			X	
3	Rb-Vilmos	X	X		X		X	
4	Rb-Manó-Polyánka	X			X		X	
5	Rb-Szulfosók				X			
6	HOM-17659	X	X	X			X	
7	MÁFI-10947	X	X	X			X	
8	MAFI-uj				X	X		
9	Szabadbattyán I		X	X	X			
10	Szabadbattyán II		X	X			X	
11	Martonyi-1	X	X	X			X	
12	Martonyi-2	X	X	X	X		X	
13	Mszi_1				X	X		
14	Mszi_6		X		X	X		
15	Mszi_7	X	X		X	X		
16	Mh1	X	X		X	X		
17	Mh2	X	X	X	X	X	X	X
18	Mh3	X				X		
19	Meleg-hegy 4	X	X	X	X	X		
20	Meleg-hegy okkerek	X	X	X	X		X	

The samples originate from three different mineral and rock collections in Hungary:

- The collection of the Institute of Mineralogy and Geology of the University of Miskolc
- Mineral collection of the Herman Ottó Museum, Miskolc
- Mineral collection of the Hungarian Geological Institute (formerly MÁFI), Budapest

As we do not collected the samples in the field, it was only possible to identify their origin to extent of the data recorded in their labels. In many cases, antimony-bearing phases are very rare, so field collection would not have been sufficiently efficient or possible because

all of the areas to be investigated are completely overburdened, or only wastedumps. Nevertheless, another important aspect was that the specimens in the collections were pre-identified, making it much easier for my studies to select specimens that also potentially enclosed antimony-bearing phases.

4. Results

4.1. Meleg hill

The samples from the Meleg hill in Lovasberény are mainly quartz and calcite containing varying amounts of pyrite/marcasite, various iron oxides, sphalerite, anglesite, acanthite, electrum and gold as accessory minerals.

Table 4 shows the antimony-bearing minerals have been identified from the area (Papp & Zajzon, 2020).

4. Table - Antimony-bearing minerals from the Meleg hill

Name	Chemical composition
stibnite	Sb_2S_3
Bi-bearing stibnite	$Sb_{1.6–1.9}Bi_{0.1-0.4}S_3$
tetrahedrite-Cu	$Cu_6(Cu_{3.75–3.81}Ag_{0.19–0.25}Cu_{1.19–1.66}Zn_{0.05–0.17})Sb_{3.45–3.73}As_{0.05–0.29}S_{13}$
jasrouxite	$Cu_{0.96–1.08}Ag_{14.56–14.63}Pb_{4.06-4.11}(Sb_{24.64–27.76}As_{15.25–15.34})S_{72}$
Bi-bearing jasrouxite	$Cu_{0.69–0.80}Ag_{14.51–14.61}Pb_{4.08–4.12}(Sb_{24.65–24.85}Bi_{0.15–0.18}As_{15.05–15.43})S_{72}$
ferdowsiite	$Cu_{0.02–0.03}Ag_{7.73–7.89}Pb_{0.14–0.22}Sb_{4.94–5.20}Bi_{0.16–0.19}As_{2.35–2.51}S_{16}$
andorite VI	$Ag_{1.01–1.12}Cu_{0–0.07}Pb_{0.74–0.86}Zn_{0–0.01}Hg_{0–0.01}Fe_{0–0.01}Sb_{2.26–2.68}Bi_{0.11–0.35}As_{0.11–0.46}S_6$
roshchinite	$Ag_{16.68–17.71}Cu_{0–1.04}Pb_{10.28–10.55}Zn_{0–0.15}Hg_{0–0.15}Fe_{0–0.07}Sb_{39.41–40.22}Bi_{5.26–5.74}As_{5.734–6.13}S_{96}$
zinkenite	$Pb_{8.60–9.26}Bi_{0.61–0.73}As_{3.54–3.83}Sb_{18.13–19.25}S_{42}$
plagionite	$Ag_{0.18–0.28}Pb_{4.74–4.96}As_{0.52–0.87}Sb_{7.3–7.93}S_{17}$
veenite	$Ag_{0.01–0.02}Pb_{1.95–2.02}As_{0.52–0.64}Sb_{1.16–1.32}S_5$
sorbyite	$Ag_{0.85–0.99}Pb_{15.60–16.41}As_{3.61–4.01}Sb_{14.65–15.86}S_{49}$
pyrargyrite/pyrostilpnite	$Ag_{2.80–3.11}Sb_{0.95–1.03}Fe_{0.01–0.06}S_3$
stibiconite/senarmontite	Sb_2O_3
schafarzikite	$FeSb_2O_4$
tripuhyite	$FeSbO_4$
oxyplumboroméite/ rosiaite/	PbSb-oxide
	PbFeAsCu(Sb)-oxide
	PbFeSbAsAg-oxide
	FeCuAsAgSbPb-oxide
	SbPbAg-oxide

It can be seen that the antimony-bearing minerals in the area are mainly sulphide and sulphosalt phases as previously described, but oxides also occur in some certain locations. The oxides are the result of post-alteration, as evidenced by the post-stibnite pseudomorphs found in the sample „Meleg-hegy okkerek”.

The area shows a great diversity of sulphide and sulphosalt minerals. The Me^{+} (Ag + Cu), Me^{2+} (Pb + Zn + Fe + Hg) and Me^{3+} (Sb + Bi + As)) triangular diagram in **Figure 2** shows the differently charged cations in the sulphide and sulphosalt phases identified in the measurements. This makes it easy to group the minerals.

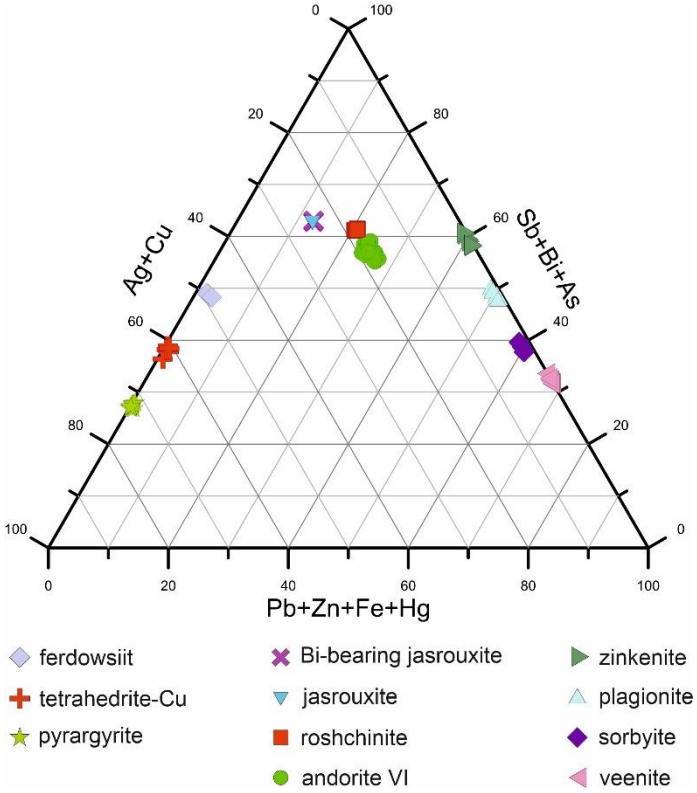

2. Figure - The (Ag_2S + Cu_2S) – (Sb_2S_3 + Bi_2S_3 + As_2S_3) – (PbS + HgS + FeS + ZnS) (at%) triangual diagram of the sulphosalt minerals identified at the Meleg hill. The diagram shows the chemical differences between the identified phases

4.2. Szabadbattyán

The samples from Szabadbattyán are composed of quartz, calcite, galena and anglesite. In addition to these, the grains also contain cerussite, various micas, covellite, calcocite, PbCu-oxides and PbCu-sulphates as accessory phases.

Four of the antimony-bearing phases have been identified, but none of them are sulphide or sulphate (**Table 5**).

5. Table - Antimony-bearing minerals from Szabadbattyán

Name	**Chemical composition**
litharge / massicote	$Pb_{0.96}Cu_{0.01}Sb_{0.01}O_1$
rosiaite	$Pb_{1.97}Sb_{2.14}O_6$
oxyplumboroméite	$Sb_{2.42–2.65}Pb_{2.29–2.59}Fe_{0.46–0.48}Cu_{0.06–0.37}S_{0.06–0.03}O_{14}$ $Pb_{1.86–2.19}Sb_{1.11–1.94}Cu_{0.66-1.25}Fe_{0.25–0.42}S_{0.27-0.66}O_7$
unknown phase	$Pb_{2.87–3.59}Cu_{2.01–2.68}S_{1.82–2.02}Sb_{0.89–1.21}Fe_{0.17–0.26}Ag_{0.00–0.02}O_{13}$

The PbO mineral (litharge/massicot) listed on the table is also indicated, but its antimony content is negligible (0-0.91 Ox%).

For SbPb-oxides, phase identification is difficult due to compositional variations, and the minerals identified as oxyplumboroméite are therefore listed with two formulas. In addition, one SbPb-oxide is listed in the table as an unidentified phase, which could not be determined from its composition as measured by electron microprobe.

The problems in the mineralogical identification originate from the heterogeneity of the individual mineral grains. These phases are typically found around anglesite and are associated with hydrothermal alteration during their formation.

4.3. Mátraszentimre

The studied samples from Szabadbattyán are composed of quartz or galena. The ore minerals are galenite, sphalerite, chalcopyrite, stibnite, arsenopyrite. Other components found in the samples are pyrite/marcasite, siderite, dolomite, ankerite and anglesite.

The antimony-bearing minerals in the area are dominated by sulphosalts along with stibnite (**Table 6**). Antimony oxide was not identified.

6. Table - Antimony-bearing minerals from Mátraszentimre

Name	**Chemical composition**
stibnite	Sb_2S_3
andorite IV	$Ag_{0.8–0.9}Pb_{1.05–1.12}Zn_{0.03–0.10}Cd_{0–0.2}Sb_{2.82–2.94}As_{0.01–0.04}S_6$
andorite VI	$Ag_{0.87–0.93}Pb_{0.91–0.95}Zn_{0.02–0.1}Fe_{0–0.02}Sb_{2.86–2.95}As_{0–0.03}S_6$
boulangerite	$Fe_{0.0-0.2}Cu_{0.0–0.03}Zn_{0.34–0.47}Pb_{5.07–5.13}Sb_{3.85–3.89}S_{11}$
rozhdestvenskayaite-Zn	$Ag_{10.47–10.81}Fe_{0.0–0.1}Zn_{1.72–2.12}As_{0.29–0.39}Sb_{3.91–4.12}S_{13}$
tetrahedrite-Zn	$Fe_{0.0–0.03}Ag_{0.0–0.03}Zn_{1.36–1.47}Cu_{10.32–10.71}Sb_{3.68–4.02}S_{13}$
tetrahedrite-Fe	$Pb_{0.00–0.02}As_{0.03–0.08}Fe_{1.56–1.74}Cu_{10.18–10.35}Sb_{3.71–3.79}S_{13}$
tennantite-Fe	$Zn_{0.02–0.08}Fe_{1.58–1.47}Cu_{10.18–10.30}Sb_{1.00–1.20}As_{2.92–3.06}S_{13}$
tennantite-Zn	$Fe_{0.03–0.13}Zn_{1.38–1.46}Cu_{10.32–10.45}Sb_{1.12–1.16}As_{2.97–3.19}S_{13}$
tennantite-Fe-Hg-Cu	$Fe_{0.24–0.34}Hg_{0.36–0.37}Cu_{10.24–10.39}Sb_{1.04–1.14}As_{2.91–3.15}S_{13}$
berthierite	$Fe_{0.99–1.03}Sb_{1.97–2.01}S_4$

In terms of sulphosalt minerals, the area is dominated by minerals of the tetrahedrite group. The chemical diversity of these minerals is impressive. Typically, iron- and zinc-dominant phases are found alongside copper, with the occasional occurrence of tennantite with a high mercury content. In addition, silver-dominant species of the tetrahedrite group are also presented (rozhdestvenskayaite-Zn) and minerals of the andorite group (andorite IV-VI) also occur. The Me^{+} (Ag + Cu), Me^{2+} (Pb + Zn + Fe + Hg) and Me^{3+} (Sb + Bi + As) triangular diagram **Figure 3** shows the differently charged cations in the sulphide and sulphosalt phases identified in the measurements.

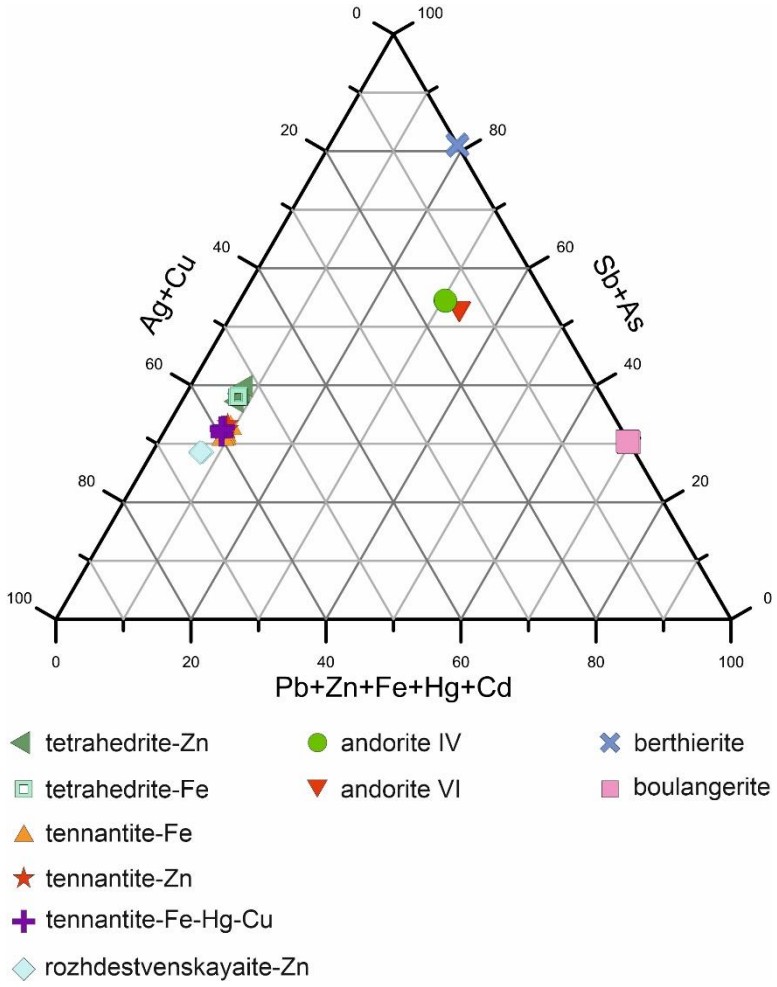

3. Figure - The (Ag_2S + Cu_2S) – (Sb_2S_3 + Bi_2S_3 + As_2S_3) – (PbS + HgS + FeS + ZnS) (at%) triangual diagram of the sulphosalt minerals identified at Mátraszentimre. The diagram shows the chemical differences between the identified phases

4.4. Rudabánya

The matrix of the Rudabánya samples is quartz, calcite, siderite and galena. In addition to these, chalcopyrite, sphalerite and Fe-oxides (hematite, goethite) were found as ore minerals, and pyrite/marcasite, anglesite, barite, cerussite, hematite, goethite, dolomite and various micas were identified as other accessory and gangue minerals.

With regard to antimony-bearing phases, Sb-sulphide, Sb-sulphosalts and various Sb-oxides are found in Rudabánya, but species-level identification of the oxides was not possible from the available sample material (**Table 7**).

7. Table - Antimony-bearing minerals from Rudabánya

Name	Chemical composition
stibnite	Sb_2S_3
diaphorite	$Ag_{3.05–3.08}Pb_{1.88–1.95}Sb_{3.08–3.14}S_8$ $Fe_{0–0.03}Zn_{0–0.46}Ag_{3.02–3.08}Pb_{1.92-2.04}Sb_{2.93–3.02}S_8$
tetrahedrite-Zn	$Ag_{0.06–0.07}Fe_{0.65–0.7}Zn_{0.88–0.93}Cu_{10.17–10.45}Bi_{0.01–0.02}As_{0.05–0.24}Sb_{0.60–0.85}S_{13}$
tennantite-Fe	$Ag_{0.02–0.03}Zn_{0.53–0.56}Fe_{1.11–1.23}Cu_{10.11–10.32}Sb_{1.48–1.57}As_{2.31–2.35}S_{13}$
geocronite	$Ag_{0–0.05}Fe_{0.02–0.05}Pb_{13.80–14.14}As_{1.92–2.03}Sb_{3.62–3.75}S_{23}$ $Cu_{0–0.03}Ag_{0–0.04}Pb_{13.86–14.08}As_{1.79–2.17}Sb_{3.59–3.78}S_{23}$ $Pb_{12.64–13.21}As_{0.10–0.15}Sb_{6.41–6.82}S_{23}$
jordanite	$Ag_{0–0.09}Zn_{0–0.02}Fe_{0.01–0.04}Bi_{0.02}Pb_{13.43–13.66}Sb_{0.41–1.05}As_{4.68–5.29}S_{23}$
pyrargyrite / pyrostilpnite	$Zn_{0.03–0.07}Cu_{0.03–0.16}Hg_{0.38–0.45}Ag_{2.37–2.73}As_{0.15–0.21}Sb_{0.75–0.86}S_3$ $Zn_{0–0.02}Pb_{0–0.07}Ag_{2.98–3.12}Sb_{0.99–1.04}S_3$
falkmanite	$As_{0–0.04}Pb_{2.85–3.13}Sb_{1.88–2.09}S_6$
stibiconite / senarmontite	Sb_2O_3
rosiaite / oxyplumboroméite	PbSb-oxid

The table shows that several mineral species have been identified in several samples (geochronite, diaphorite, pyrargyrite/pyrostilpnite), which are described as one mineral species but are well distinguishable from each other in terms of their chemical composition.

The Me^+ (Ag + Cu), Me^{2+} (Pb + Zn + Fe + Hg) and Me^{3+} (Sb + Bi + As) triangular diagram **Figure 4** shows the differently charged cations in the sulphide and sulphosalt phases identified in the measurements.

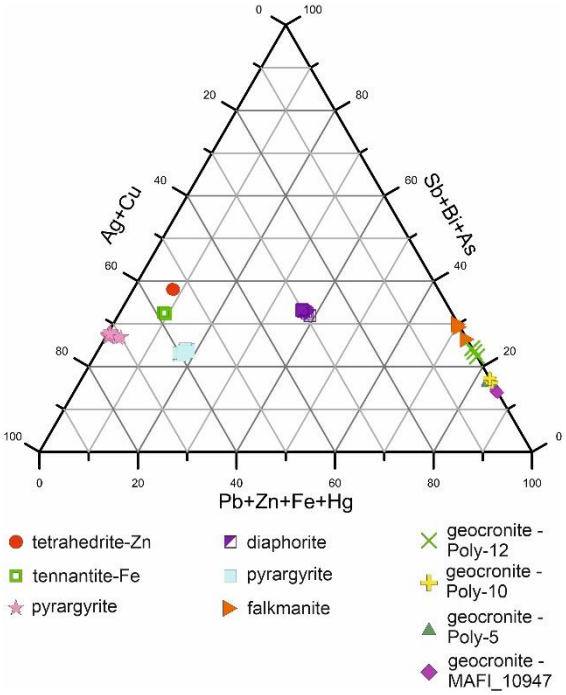

4. Figure - The (Ag_2S + Cu_2S) – (Sb_2S_3 + Bi_2S_3 + As_2S_3) – (PbS + HgS + FeS + ZnS) (at%) triangual diagram of the sulphosalt minerals identified at Rudabánya. The diagram shows the chemical differences between the identified phases

4.5. Martonyi

Samples from the Martony area are composed of quartz, galena and anglesite, and contain large amounts of sphalerite, pyrite/marcasite, various carbonates (calcite, dolomite, siderite, cerussite), Fe-Mn oxides (hematite, goethite, pyrolusite, cryptomelane), feldspars, barite and cinnabarite.

The minerals identified as antimony-bearing phases are listed in **Table 8** (Papp, 2020):

8. Table - Antimony-bearing minerals from Martonyi

Name	**Chemical composition**
sibnite	Sb_2S_3
boulangerite	$Pb_{5.27–5.35}\ Zn_{0–0.19}Fe_{0–0.05}Sb_{3.73–3.85}S_{11}$
boulangerite	$Cu_{0–0.01}Fe_{0–0.02}Zn_{0–0.03}Pb_{5.07–5.60}Sb_{3.76–3.93}S_{11}$
diaphorite	$Ag_{2.89–2.96}Cu_{0.03}\ Pb_{1.87–2.05}\ Hg_{0.13–0.14}Fe_{0.03–0.15}Sb_{2.90–2.94}S_8$
Fe-bearing diaphorite	$Ag_{2.59–2.83}Cu_{0.01–0.06}\ Pb_{1.69–1.76}\ Fe_{0.49–0.72}Hg_{0.0.9–0.12}Sb_{2.54–2.79}S_8$
freieslebenite	$Ag_{0.97.99–1.03}\ Cu_{0.01–0.02}Pb_{1.06–1.1}Hg_{0.03–0.05}\ Sb_{0.99–1.03}S_{3.00}$
stibiconite / senarmontite	Sb_2O_3

The (Me^+ (Ag + Cu), Me^{2+} (Pb + Zn + Fe + Hg) and Me^{3+} (Sb + Bi + As)) triangular diagram **Figure 5** shows the differently charged cations in the sulphide and sulphosalt phases identified in the measurements.

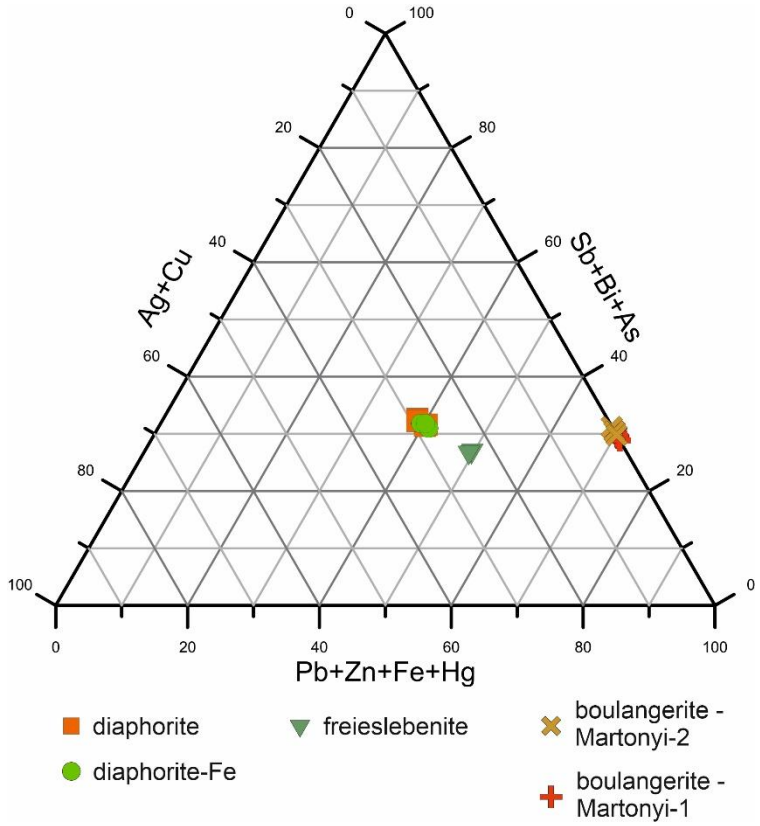

5. Figure - The (Ag_2S + Cu_2S) – (Sb_2S_3 + Bi_2S_3 + As_2S_3) – (PbS + HgS + FeS + ZnS) (at%) triangual diagram of the sulphosalt minerals identified at Martonyi. The diagram shows the chemical differences between the identified phases

4.6. Andorite minerals from Hungary

During my work, I was able to identify four different andorite minerals in two Hungarian deposits – Meleg Hill and Mátraszentimre.

Based on the analytical data, the andorite homologue value (N) and the substitution percentage (L%) calculations, three different types of andorite-series minerals with four chemical compositions can be distinguished in the sample from Meleg Hill with the following average compositions and values:

- andorite VI – $Ag_{1.06}Cu_{0.04}Pb_{0.8}Sb_{2.49}Bi_{0.22}As_{0.3}S_6$; N = 4.17; L% = 107.07
- Bi-bearing jasrouxite – $Ag_{14.57}Cu_{0.74}Pb_{4.1}Sb_{24.75}Bi_{0.17}As_{15.27}S_{72}$; N = 3.79; L% = 137.41
- jasrouxite – $Ag_{15.30}Cu_{1.02}Pb_{4.08}Sb_{24.71}As_{15.30}S_{72}$; N = 3.90; L% = 135.07
- roshchinite – $Ag_{17.23}Cu_{0.53}Pb_{10.4}Hg_{0.04}Zn_{0.04}Fe_{0.02}Sb_{39.73}Bi_{5.52}As_{5.98}S_{96}$; N = 3.70; L% = 121.41

In the samples from Mátraszentimre, I was able to identify andorite IV and andorite VI minerals:

- andorite IV – $Ag_{13.75}Pb_{17.21}Zn_{0.87}Cd_{0.04}Sb_{46}As_{0.34}S_{96}$; N = 3.80; L% = 93.64
- andorite VI – $Ag_{0.90}Pb_{0.93}Zn_{0.06}Fe_{0.01}Sb_{2.91}As_{0.02}S_6$; N = 3.75; L% = 101.29

The theoretical homologue value for the lillianite-group minerals is N = 4, but in the case of the andorite series, it may deviate from 4 due to the element substitution in the different sites. In the andorite VI grains from Meleg Hill the Me^{2+} cation Pb is undersubstituted and the Me^{3+} cation Sb is replaced with minor Bi and As compared to the theoretical composition ($Ag^{+}Pb^{2+}Sb^{3+}{}_3S_6$). In the roshchinite and jasrouxite grains, the Me^{2+} and Me^{3+} cations are oversubstituted, and the Me^{+} is undersubstituted (the theoretical composition for roshchinite is $Ag^{+}{}_{19}Pb^{2+}{}_{10}Sb^{3+}{}_{51}S_{96}$ and for jasrouxite is $Ag_{16}Pb_4(Sb_{24}As_{16})S_{72}$). In this case, higher Bi-As-replacement can be observed.

Based on the measured wt% of the Me^{+}, Me^{2+} and Me^{3+} cations, three different kinds of minerals can be distinguished in the Meleg Hill samples and two from Mátraszentimre (**Figure 6–7**). The chemical composition of roshchinite from Meleg Hill is similar to the sample studied by Makovicky, et al. (2018) and is close to the ideal chemical composition of the species. It defines a well distinguishable range on both of the diagrams (**Figure 6,** encircled in green; **Figure 7,** green band) as well as the jasrouxite (**Figure 6,** encircled in red; **Figure 7,** red band). In **Figure 7** there is also a well-defined range of andorite VI (purple band) that includes the results of this study, Pršek, et al. (2009), Pažout, (2017), Moëlo et al. (1984) and the ideal andorite VI. In **Figure 6** andorite VI group (purple circle) overlap with the ideal arsenquatrandorite and with the andorite IV and fizélyite measurements of PAŽOUT (2017). The original results of Pažout, (2017) show four separate groups of the andorite VI, andorite IV, ramdohrite and fizélyite (**Figure 6**, encircled in blue).

In the case of the samples of Pršek, et al. (2009) the difference between the ideal positions of the andorite-series minerals and the measured data on the ternary diagram is caused by the Bi-As-substitution and the low Me^{2+} content of the samples.

The formerly used comparative ternary diagrams of the system ($Ag_2S + Cu_2S$)–($Sb_2S_3 + Bi_2S_3 + As_2S_3$)–(PbS + HgS + FeS + ZnS + CdS) and the Bi / (Bi + Sb) (at%) vs andorite substitution $(Ag,Cu)^{+} + (Sb,Bi,As)^{3+} \leftrightarrow 2\ (Pb,Hg,Fe,Zn,Cd)^{2+}$ plot of andorite-series minerals are not adequate enough to separate the species from each other, due to the highly variable element substitution in the case of Me^{+}, Me^{2+} and Me^{3+} cations.

Calculation of the andorite substitution percentage (L%) and the homologue order value (N), with their combined representation on the two diagrams is always necessary to distinguish the mineral species.

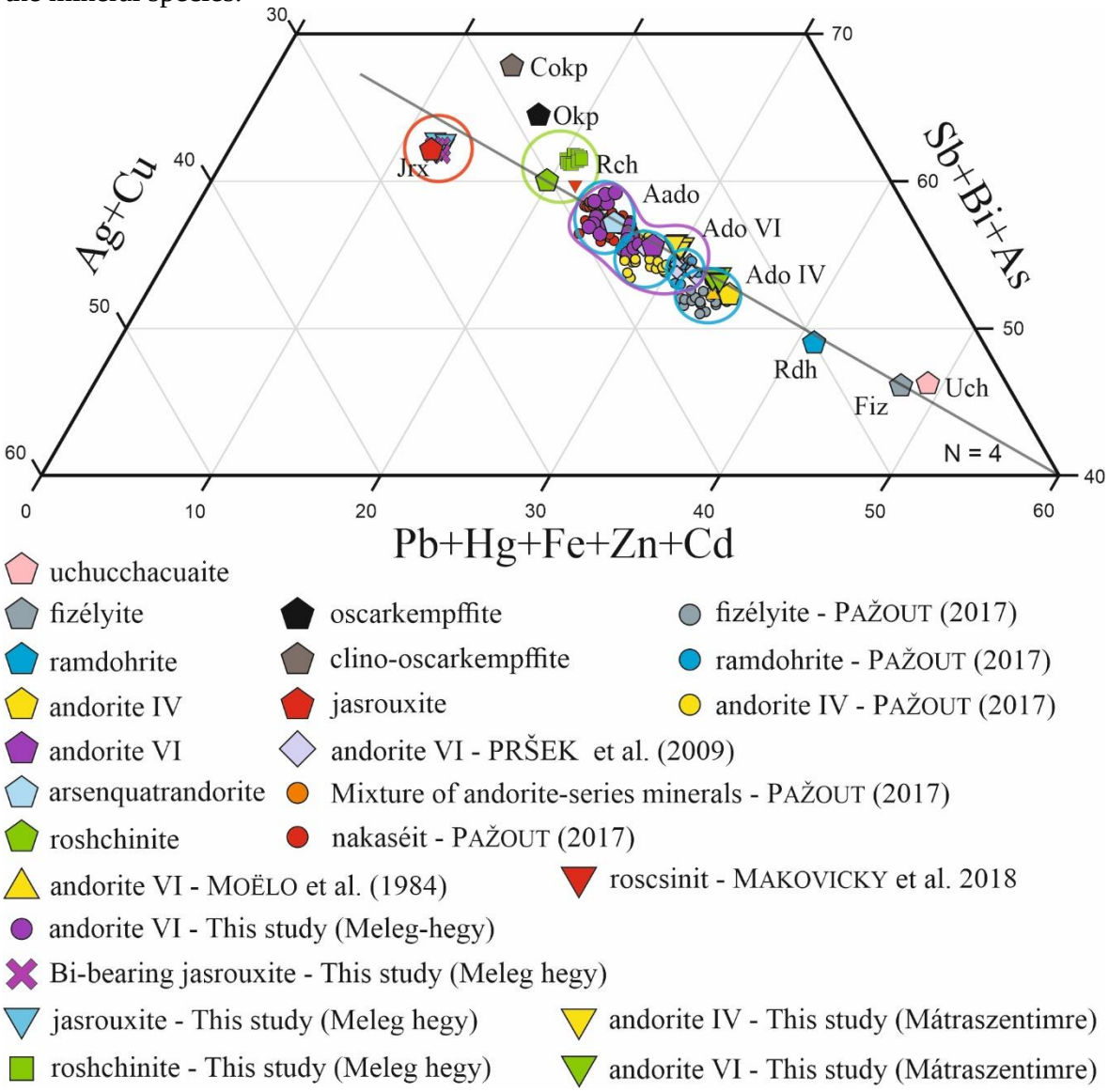

6. Figure - Ternary diagram of the (Ag_2S + Cu_2S)–(Sb_2S_3 + Bi_2S_3 + As_2S_3)–(PbS + HgS + FeS + ZnS + CdS) showing the andorite substitution $(Ag,Cu)^{+}$ + $(Sb,Bi,As)^{3+}$ ↔ 2 $(Pb,Hg,Fe,Zn,Cd)^{2+}$ (andorite series) in 58 measurements from this work and from other authors based on Pažout, (2017). Pentagons: members of the andorite-series minerals with ideal chemical composition; Encircled in blue: field of the andorite-series minerals based on the results of Pažout, (2017); Encircled in green: field of roshchinite (Rch) based on results of this study and Makovicky, et al. (2018); Encircled in purple: field of andorite VI based on the results of this study and Pršek, et al. (2009); – N: andorite homologue value; Jrx: jasrouxite, Cokp: clino-oscarkempffite, Okp. oscarkempffite, Rch: roshchinite, Aado: arsenquatrandorite Ado VI: andorite VI, Ado IV: andorite IV, Rdh: ramdohrite, Fiz: fizélyite, Uch: uchucchacuaite; mineral symbols after Warr (2021)

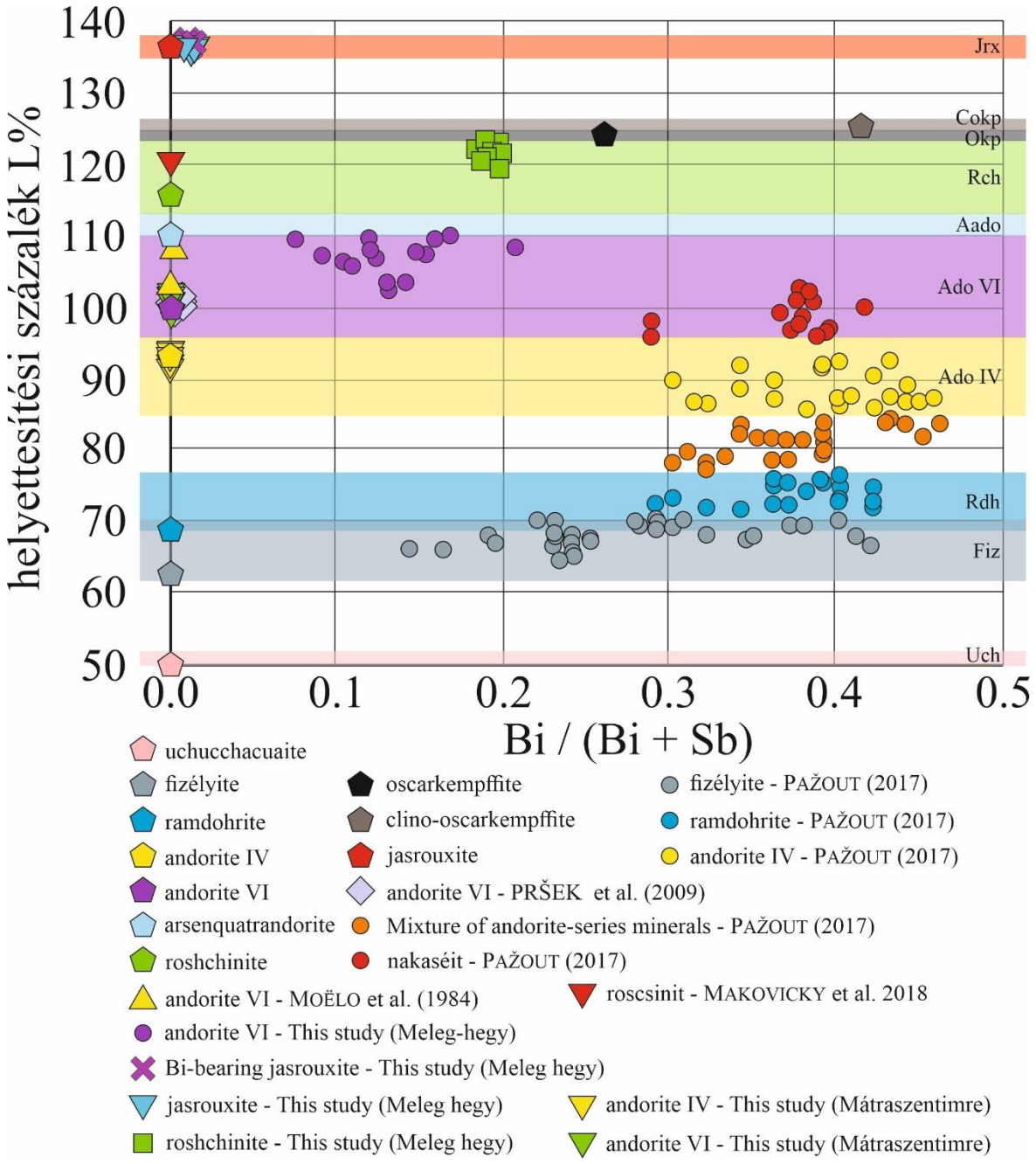

7. Figure - The Bi / (Bi + Sb) (at%) *vs* andorite substitution $(Ag,Cu)^{+} + (Sb,Bi,As)^{3+} \leftrightarrow 2\ (Pb,Hg,Fe,Zn,Cd)^{2+}$ plot of andorite-series minerals with 58 measurements from this work and from other authors based on PAŽOUT (2017). The plot shows the ideal (andorite VI), the undersubstituted (uchucchacuaite, fizélyite, ramdohrite and andorite IV) and oversubstituted (arsenquatrandorite, roshchinite, oscarkempffite, clino-oscarkempffite and jasrouxite) members of the andorite series with pentagons. The colour bands represent the fields of the species. Jrx: jasrouxite, Cokp: clino-oscarkempffite, Okp. oscarkempffite, Rch: roshchinite, Aado: arsenquatrandorite Ado VI: andorite VI, Ado IV: andorite IV, Rdh: ramdohrite, Fiz: fizélyite, Uch: uchucchacuaite; mineral symbols after Warr (2021)

5. Raman spectroscopy

Raman spectroscopy measurements were performed for the Mh2 sample at and around the EPMA measurement points in homogeneous, contiguous areas of the same shade of grey. The aim of the study was to verify the presence of crystals of 5-50 µm size in the Mh2 sample, identified as andorite VI, roshchinite and ferdowsiite on the basis of chemical composition, to check whether the chemical differences are indeed due to the presence of different mineral species.

The identification of the crystals was hindered by the fact that Raman spectra were only available for andorite VI from reference databases and literature data, and not for roshchinite and ferdowsiite. Although the species identification of the latter could not be made on the basis of Raman spectroscopy alone, the spectra from areas with different chemical compositions were varied according to the different species identified as crystals by electron microprobe analysis (**Figure 8**). In addition to the spectral variations, the laser beam used for the analysis of the other two phases also affected the measured areas, The andorite VI spectra examined at different points in the sample show a variable slope depending on the orientation.

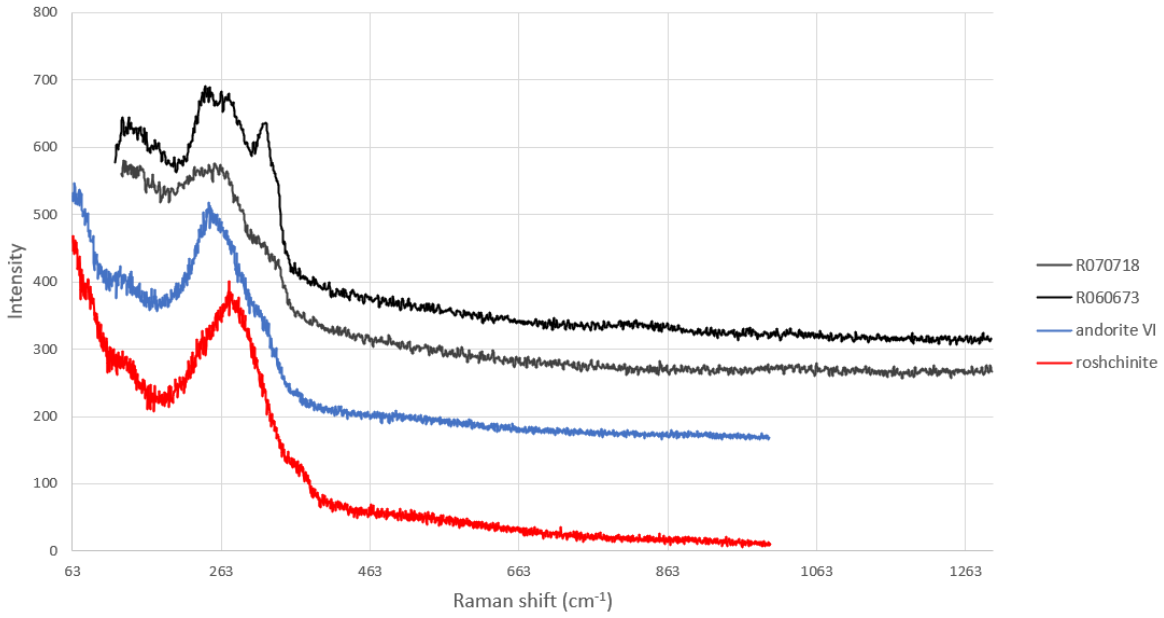

8. Figure - The Raman spectra of andorite VI and roshchinite identified in the sample compared to the andorite VI spectrum in the RRUFF database

6. Categorization of antimony-bearing deposits in Hungary

Economically exploitable antimony deposits are geologically limited to a narrow genetic environment. Most of them are typically formed by hydrothermal processes in volcanic or sub-volcanic areas. In terms of their formation temperature, they are formed in epithermal zones, in areas away from the magmatic body. The deposits are generally associated with acidic and intermediate magmatic (granite, granodiorite, monzonite, diorite) intrusions formed at higher temperatures (Kiss, 1982a; 1982b; Dill, 2010; Laznicka, 2010).

In terms of mineral composition, two major types can be distinguished:

- monomineralic ore deposits: typically composed only of antimony minerals, mostly stibnite,
- complex antimony deposits: in addition to antimony, these deposits also contain large quantities of several other metals (Hg, Pb, Cu, As, Bi, W).
-

Sb ore deposits can be classified into 14 different groups in terms of their appearance (Dill, 2010; Földessy & Less, 2013):

1. Magmatic antimony deposits:
   1.1. Granite-related vein-type (and replacement) deposits
      1.1.1. Sb-W
      1.1.2. Sb-Pb-Cu-Zn-As
      1.1.3. Sb-Hg-W-Ba
   1.2. Skarn-type Sb-(Au-Hg-As) deposits (Sarawak-type)
   1.3. Carbonate-hosted disseminated Sb-Au-Ag deposits (Carlin-type)
   1.4. Shallow high- (HS) and low-sulfidation (LS) Sb deposits
   1.5. Near-surface low-sulfidation-type Sb–(Hg) deposits
   1.6. Sb deposits related to (ultra)basic rocks and greenstone belts
2. Structure-related antimony deposits
   2.1. Shearzone-hosted, mesothermal (Au)-Sb veins
      2.1.1. Monotonous Sb deposits
      2.1.2. Polymetallic Sb–(Au–W–Sn–As–Zn–Pb) deposits
3. Sedimentary antimony deposits
   3.1. Stratabound deposit (with remobilization)
      3.1.1. Monotonous sedimentary-diagenetic Sb deposit
      3.1.2. Hg–Sb–(W) deposits in carbargillites and graphite schists
      3.1.3. Polymetallic Sb mineralization in black shales (alum shales)
   3.2. Sb-enriched coal seams

6.1. Meleg hegy

The Meleg Hill in the Velence mountains is an Sb-As-Ag-(Au) indication in the siliceous breccia off the Paleogene volcanics. Similar paragenesis and formation age analogy in the Carpathian and Alpine ranges is not known.

According to Dill (2010) the Meleg hill belongs to the group of magmatic antimony deposits (1) within the 1.1. Shallow high- (HS) and low-sulfidation (LS) Sb deposits (1.4). According to Dill (2010), this group includes late kainozoic HS porphyritic and epithermal copper-gold deposits and sulphide ores that were formed during magma deposition along fault zones. Examples include the Cosuño and Milluri antimony deposits in the Bolivian Andes. Here, significant clay mineralisation, silicious alteration, kaolinisation and other alterations can be observed. In the near-surface zones of the deposits, low-temperature hydrothermal processes have led to the formation of antimony sulphides and sulphosalts. Dill (2010) also includes the LS gold-silver ore deposit at Kremnica in this group, with the comment that the site does not fully meet the site criteria.

From the geological point of view, the ore deposits of the Meleg Hill are geologically related to the areas of Szabadbattyán, Rudabánya and Martonyi. According to literature (Benkó, et al., 2010; 2014a; 2014b; Hargitainé Molnár, 2019) during the formation of these ore bodies, the starting point of the initial plate fragments may have been the Central-Southern Alps and they were displaced to their present position along the Periadriatic-Balaton Lineament and the Darnó Zone. In terms of the parageneses identified in my work, there is no relationship

among the areas, they show a very different mineral assemblages. The closest relationship has been identified are between the Szabadattyán and Meleg Hill areas, but elemental enrichments found in two areas do not strongly support this connection. While there is a well-traced presence of bismuth in the Meleg Hill minerals (Bi-zonated stibnite, bismuth-bearing andorite VI, roshschinite, jasrouxite and ferdowsiite), this is not evident in the samples from Szabadattyán. Based on Bi content, the hydrothermal solutions from Meleg Hill had higher temperature. The formation ages of the two areas (Triassic and Paleogene) are also different.

In the mineral assemblages of the studied areas, I identified a relationship only with the Mátraszentimre deposit. Both sites contain andorite and tetrahedrite minerals, but in the case of Mátraszentimre the absence of bismuth and the significant copper dominance, as shown by the identified mineral association (tetrahedrite-tennantite), are not negligible.

6.2. Szabadbattyán

Based on the classification of Dill (2010) Szabadbattyán belongs to the group of Structure-related antimony deposits (2) within the Polymetallic Sb–(Au–W–Sn–As–Zn–Pb) deposits (2.1.2.) group. These ore deposits are typically formed along shear zones due to techtonic plate movements during Variscan mountain range formation and are characterised by long-lived, multi-phase hydrothermal alteration. Complex Pb-Sb sulphosalts are common, as are vein-network-associated ore deposits along fractures.

The closest local connection of the Szabadbattyán area is commonly referred to the lead ore deposit on the Meleg Hill (Benkó, et al., 2010; 2014a; 2014b; Hargitainé Molnár, 2019), as both sites are located along the Periadriatic-Balaton Lineament, only a few tens of kilometres apart. The ore bodies of Rudabánya and Martonyi, which belong to the same fault line above the Darnó zone, also belong to this system.

In addition to the genetic similarities, the mineral assemblages at Martonyi and Rudabánya are also partly analogous to the paragenesis at Szabadbattyán, with different carbonate and sulphate phases (calcite, siderite, cerussite, anglesite), galena, sphalerite and non-ferrous oxides appearing at all three sites. Among the samples I have studied, the Rb-Mano-Polyanka from Rudabánya shows oxyplumboroméite-like minerals that are very similar to the SbPb-oxide phases found in the Szabadbattyán II sample, which also indicates similar ore-forming processes and formation environments.

6.3. Mátraszentimre

According to Dill (2010) the Mátraszentimre belongs to group of magmatic antimony deposits (1) within the 1.1. Shallow high- (HS) and low-sulfidation (LS) Sb deposits (1.4).

Among the sites I have studied, a mineralogical relationship can also be identified with the Meleg Hill orebody, but the orebody at Mátraszentimre is younger. Although the similarity of the paragenesis (andorite series minerals, tetrahedrite, stibnite) is important, significant copper enrichment can be identified here, but the presence of bismuth is not detectable in the area. For this reason, it is likely that the parts of the Mátraszentimre deposit that I have studied are the result of lower temperature hydrothermal processes.

6.4. Rudabánya

Based on the classification of Dill (2010) Rudabánya belongs to the group of Structure-related antimony deposits (2) within the Polymetallic Sb–(Au–W–Sn–As–Zn–Pb) deposits (2.1.2.) group.

Among the areas I have studied, there is a clear and direct link with the Martonyi ore deposit, which is also located in the Darnó zone at the north-eastern end of the Rudabánya Mountains. The two areas are related both in terms of their formation and their paragenesis. The antimony-bearing mineral phases I studied were formed during the last Ag-As-Cu-Hg-Sb phase of the secondary ore formation processes described by Leskó et al. (2020) in some cases by remobilization of pre-existing ores. This result is also consistent with the processes described in the work of Szakáll (2001).

In terms of mineral association, a relationship between the Rudabánya and Szabadbattyán can also be found. Both areas are characterised by carbonates, dolomitisation and iron metasomatism, and are also located along the periadriatic line, related to the central and southern Alps. Although, the ore body in the Szabadbattyán area was intruded into an older limestone, hydrothermal processes have developed very similar paragenesis. A number of other carbonate and sulphate minerals are associated with the galenite-sphalerite-type Pb-Zn-ore deposits. In both cases antimony-containing solutions produced PbSb-oxides (Szabadbattyán II, Rb-Manó-Polyánka samples).

6.5. Martonyi

Based on the classification of Dill (2010) Martonyi belongs to the group of Structure-related antimony deposits (2) within the Polymetallic Sb–(Au–W–Sn–As–Zn–Pb) deposits (2.1.2.) group.

7. Theses

Thesis 1*: I identified the first andorite minerals at species level in Hungary using different crystal chemistry parameters andorite homologue value and substitution percentage. Andorite VI, jasrouxite and roshchinite mineral species from the Meleg Hill, Velence Mts and andorite VI and andorite IV mineral species from Mátraszentimre were described.*
I complemented the grouping scheme of Pažout (2017) with roshchinite and jasrouxite and showed that in some cases the original grouping method is not adequate, due to different substitutions of Me^{+} *and* Me^{2+} *and* Me^{3+} *cations.*

Thesis 2: *I described a total of eight different complex sulphosalt mineral species that have not been previously known from Hungary: andorite IV, andorite VI, diaphorite, firdawsiite, jasrouxite, jordanite, roshchinite and rozhdestvenskayaite-(Zn).*

Thesis 3: *I applied the current tetrahedrite grouping system defined by Biagioni et al. (2020) first in Hungary to identify the measured phases at species level. I was able to distinguish the mineral species rozhdestvenskayaite-(Zn), tennantite-Fe, tennantite-Zn, tetrahedrite-Cu, tetrahedrite-Fe and tetrahedrite-Zn. I described a tennantite-Fe-Hg-Cu phase that cannot be classified in the above mentioned valid classification scheme based on the second* Me^{2+} *cation, pointing out its deficiency.*

Thesis 4: *I identified a total of 31 different antimony-bearing minerals in the five Hungarian deposits: a total of 25 sulphide minerals – of which 24 were sulphosalts – and 6 oxide phases. From the sulphosalts, for several of them this is the first description of the location:*

A. *From Meleg Hill andorite VI, firdawsiite, jasrouxite and bismuth-bearing jasrouxite, pyrargyrite/pirostilpnite, roshchinite and tetrahedrite-Cu;*
B. *From Szár Hill, Szabadbattyán rosiaite;*
C. *From Mátraszentimre andorite IV, andorite VI, rozhdestvenskayaite-(Zn), tennantite-Fe, tennantite-Zn, tennantite-Fe-Hg-Cu, tetrahedrite-Fe and tetrahedrite-Zn;*
D. *From Rudabánya diaphorite, falcmanite, tennantite-Fe and tetrahedrite-Zn;*
E. *From Martonyi diaphorite and freieslebenite.*

Thesis 5: *Based on my results, the five investigated locations can be divided into two category based on the the antimony deposit grouping system of Dill (2010). The ore bodies of Mátraszentimre and Meleg Hill belong to the group of magmatic antimony deposits (1) within the „Shallow high- (HS) and low-sulfidation (LS) Sb deposits (1.4)", while the deposits at Szabadbattyán, Rudabánya and Martonyi belong to the group of „Structure-related antimony deposits (2)" withnin the „Polymetallic Sb–(Au–W–Sn–As–Zn–Pb) deposits (2.1.2.)" group.*

8. List of publications related to the PhD work

Papp, R. Z. & Zajzon, N., 2018. Magyarországi szulfosó ásványok előfordulásai. In: G. Mucsi & R. Z. Papp, szerk. *Doktoranduszok Fóruma : Műszaki Földtudományi Kar szekciókiadványa.* Miskolc: Miskolci Egyetem Tudományos és Nemzetközi Rektorhelyettesi Titkárság, p. 90.

Papp, R. Z., Zajzon, N., 2018. Study on andorite IV and andorite VI from Meleg-hill, Velence Mts., and Mátraszentimre, Mátra Mts., Hungary, Abstract book of Joint 5th CEMC and 7th MSCC conferences, pp. 86–88.

Papp, R. Z., Zajzon, N., 2019. Andorite-series sulphosalts from the Meleg-hill, Velence Mst., Hungary, *Abstract book of 1st International Student Conference on Geochemistry and Mineral Deposits*, Prague, pp. 25–27.

Papp, R. Z., 2020. Sb tartalmú ásványok vizsgálata Martonyi térségéből. In: N. P. Szabó & R. Z. Papp, eds. *Doktoranduszok Fóruma: Miskolc, 2019. november 21: Műszaki Földtudományi Kar szekciókiadványa.* Miskolc: Miskolci Egyetem Tudományos és Nemzetközi Rektorhelyettesi Titkárság, p. 97.

Papp, R. Z. & Zajzon, N., 2020. Antimontartalmú szulfosók vizsgálata a velencei-hegységi Meleg-hegy térségéből. *Műszaki Földtudományi Közlemények,* Volume 89, pp. 342–346.

Papp R. Z., Topa, B. A., Zajzon, N., 2022: Study on andorite-series minerals from Meleg Hill, Velence Mts., Hungary, *Bulleting of the Hungarian Geological Society*, Volume 152/3.

9. List of literature used in the thesis book

Benkó, Zs., Molnár, F., Pécskay, Z., Németh, T. & Lespinasse, M., 2010. Genetic and age relationship of the base metal mineralization along the Periadriatic-Balaton Lineament system on the basis of radiogenic isotope studies. *Acta Mineralogica Petrographica Abstract Series,* Volume 6, p. 224.

Benkó, Zs., Molnar, F., Billström, K. & Pécskay, Z., 2014a. Triassic fluid mobilization and epigenetic lead-zinc sulphide mineralization in the Transdanubian Shear Zone (Pannonian Basin, Hungary). *Geologica Carpathica,* Volume 65/3, pp. 177–194.

Benkó, Zs., Molnár, F., Lespinasse, M. & Váczi, T., 2014b. Evidence for exhumation of a granite intrusion in a regional extensional stress regime based on coupled microstructural and fluid inclusion plane studies - An example from the Velence Mts., Hungary. *Journal of Structural Geology,* Volume 65, pp. 44–58.

Biagioni, C. George, L., Cook, N. J., Makovicky, E., Moëlo, Y., Pasero, M., Sejkora, J., Stanley, C. J., Welch, M. D. & Bosi, F., 2020. The tetrahedrite group: Nomenclature and classification. *American Mineralogis,* Volume 105, p. 109–122.

Dill, H. G., 2010. The "chessboard" classification scheme of mineral deposits: Mineralogy and geology from aluminum to zirconium. *Earth-Science Reviews,* Volume 100, pp. 1–420.

Földessy, J. & Less, G. eds., 2013. *Stratégiai fontosságú ásványi nyersanyagok II.*. Miskolc: Milagrossa Ktf.

Hargitainé Molnár, Zs., 2019. *Nyersanyagok és indikációik geológiai és ásványtani vizsgálata, különös tekintettel az Észak-Dunántúlon észlelt urán és ritkaföldfém nyomokra - Doktori értekezés.* Budapest: Eötvös Loránd Tudományegyetem Földtudományi Doktori Iskola.

Kiss, J., 1982a. *Ércteleptan I.*. Budapest: Tankönyvkiadó Vállalat.

Kiss, J., 1982b. *Ércteleptan II.*. Budapest: Tankönyvkiadó Vállalat.

Kostov, I. & Minčeva-Stefanova, J., 1981. *Sulphide Minerals - Crystal chemistry, parageneses and systematics.* Sofia: The Bulgarian Academy of Sciences.

Krenner, J. A., 1894. Andorit, ein neues ungarisches silbererz. *Zeitschrift für Krystallographie und Mineralogie,* Volume 23, pp. 497–499.

Krenner, J. S., 1892. Andorit, új hazai ezüstércz. *Mathematikai és Természettudományi értesítő,* Volume 11, pp. 119–122.

Laznicka, P., 2010. *Giant Metallic Deposits: Future Sources of Industrial Metals.* 2. ed. Berlin: Springer.

Leskó, M. Zs., Jakab, G., Móricz, F. & Kristály, F., 2020. A Martonyi vasércesedés kutatásának újabb eredményei. *Műszaki Földtudományi Közlemények,* 89(1), pp. 334–341.

Makovicky, E. & Karup-Møller, S., 1977a. Chemistry and crystallography of the lillianite homologous series. Part I. General properties and definitions.. *Neues Jahrbuch für Mineralogie,* Volume 130/3, pp. 264–287.

Makovicky, E. & Karup-Møller, S., 1977b. Chemistry and crystallography of the lillianite homologous series. Part II: Definition of new minerals: eskimoite, vikingite, ourayite, and treasurite. Redefinition of schirmerite and new data on the lillianite-gustavite solid solution series.. *Neues Jahrbuch für Mineralogie,* Volume 131, pp. 56–82.

Makovicky, E. & Karup-Møller, S., 1977c. Chemistry and crystallography of the lillianite homologous series Part III. Crystal chemistry of lillianite homologues. Related Phases. *Neues Jahrbuch für Mineralogie,* Volume 131, pp. 187–207.

Makovicky, E., Stöger, B. & Topa, D., 2018. The incommensurately modulated crystal structure of roshchinite, Cu0.09Ag1.04Pb0.65Sb2.82As0.37S6.08. *Zeitschrift für Kristallographie - Crystalline Materials,* Volume 233/3-4, pp. 255–267.

Moëlo, Y., Makovicky, E. & Karup-Møller, S., 1984. New data on minerals of the andorite series. *Neues Jahrbuch für Mineralogie,* Volume 4, pp. 175–182.

Moëlo, Y., Makovicky, E., Mozgova, Nadejda N., Jambor, J. L., Cook, N., Pring, A., Paar, W., Nickel, E. H., Graeser, S., Kraup-Moller, S., Balic-Žunic, T., Mumme, W. G., Vurro, F., Topa, D., Bindi, L., Bente, K. & Shimizu, M., 2008. Sulfosalt systematics: a review. Report of the sulfosalt sub-committee of the IMA Commission on Ore Mineralogy. *European Journal of Mineralogy,* Volume 20, p. 7–46.

Móricz, F., Mádai, F., Szakáll, S., Tompa, R. & Molnár, J.,2013. Antimon. In: G. Less, ed. *CriticEl Monográfia Sorozat 2. - Stratégiai fontosságú ásványi nyersanyagok 2.* Miskolc: Milagrossa Kft., p. 9–40.

Ozdín, D. & Sejkora, J., 2009. Andorite IV and andorite VI from the Dúbrava deposit in the Nízke Tatry Mts. (Slovak Republic). *Bulletin mineralogicko-petrologického oddělení Národního muzea v Praze,* Volume 17/1, pp. 65–68.

Papp, R. Z., 2020. Sb tartalmú ásványok vizsgálata Martonyi térségéből. In: N. P. Szabó & R. Z. Papp, eds. *Doktoranduszok Fóruma: Miskolc, 2019. november 21: Műszaki Földtudományi Kar szekciókiadványa.* Miskolc: Miskolci Egyetem Tudományos és Nemzetközi Rektorhelyettesi Titkárság, p. 97.

Papp, R. Z. & Zajzon, N., 2018. Magyarországi szulfosó ásványok előfordulásai. In: G. Mucsi & R. Z. Papp, szerk. *Doktoranduszok Fóruma : Műszaki Földtudományi Kar szekciókiadványa.* Miskolc: Miskolci Egyetem Tudományos és Nemzetközi Rektorhelyettesi Titkárság, p. 90.

Papp, R. Z. & Zajzon, N., 2020. Antimontartalmú szulfosók vizsgálata a velencei-hegységi Meleg-hegy térségéből. *Műszaki Földtudományi Közlemények,* Volume 89, pp. 342–346.

Pažout, R., 2017. Lillianite homologues from Kutná Hora ore district, Czech Republic: A 261 case of large-scale Sb for Bi substitution. *Journal of Geosciences,* Volume 62, p. 37–57.

Pouchou, J. L. & Pichoir, F., 1984. A new model for quantitative X-ray microanalysis. *Res Aerospace,* Volume 3, pp. 167–192.

Pršek, J., Lauko, L. & Valášková, M., 2009. Andorite VI from stibnite mineralization in the Spiš-Gemer Ore Mts. (Zlatá Idka, Dobšiná-Tiefengründel localities). *Mineralia Slovaca,* Volume 41, pp. 183–190.

Sawada, H., Kawada, I., Hellner, E. & Tokonami, M., 1987. The crystal structure of senandorite (andorite VI): PbAgSb3S6. *Zeitschhrift für Kristallographie,* Volume 180, pp. 141–150.

Szakáll, S., 2001. *Rudabánya ásványai. Egy régi bánya új élete.* Budapest: Kőország Kiadó.

Warr, L. N., 2021. IMA–CNMNC approved mineral symbols. *Mineralogical Magazine,* Volume 85, pp. 291–320.